

# Autonomous Robotic System for Bridge Deck Data Collection and Analysis

Hung Manh La, Nenad Gucunski, Seong-Hoon Kee, Jingang Yi, Turgay Senlet, Luan Nguyen

**Abstract**—Bridge deck inspection is conducted to identify bridge condition deterioration and, thus, to facilitate implementation of appropriate maintenance or rehabilitation procedures. In this paper, we report the development of a robotic system for bridge deck data collection and analysis. The robotic system accurately localizes itself and autonomously maneuvers on the bridge deck to collect visual images and conduct nondestructive evaluation (NDE) measurements. The developed robotic system can reduce the cost and time of the bridge deck data collection. Crack detection and mapping algorithm to build the deck crack maps is presented in detail. The electrical resistivity (ER), impact-echo (IE) and ultrasonic surface waves (USW) data collected by the robot are analyzed to generate the corrosion, delamination and concrete elastic modulus maps of the deck. The presented robotic system has been successfully deployed to inspect numerous bridges.

## I. INTRODUCTION

### A. Motivation

In the United States, there are currently more than 600,000 bridges, the condition of which is critical for the safety of the traveling public and economic vitality of the country. According to the National Bridge Inventory there are about 150,000 bridges through the U.S. that are structurally deficient or functionally obsolete. The cost of maintenance and rehabilitation of the deteriorating bridges is immense. The cost of repairing and replacing deteriorating highway bridges in U.S. was estimated to be more than \$140 billions in 2008 [1]. Condition monitoring and timely implementation of maintenance and rehabilitation procedures are needed to reduce future costs associated with bridge management. Application of nondestructive evaluation (NDE) technologies is one of the effective ways to monitor and predict bridge deterioration.

Robotics and automation technologies have increasingly gained attention for bridge inspection, maintenance, and rehabilitation. Mobile robot- or vehicle-based inspection and maintenance systems are developed for vision based crack

detection and maintenance of highways and tunnels [2]–[4]. In one case, a mobile manipulator is used for bridge crack inspection [5]. A bridge inspection system that includes a specially designed car with a robotic mechanism and a control system for automatic crack detection is reported in [6], [7]. Similar systems are reported in [8], [9] for vision-based automatic crack detection and mapping and [10] to detect cracks on a tunnel. Edge/crack detection algorithms such as Sobel and Laplacian operators are used.

Most of abovementioned works classify, measure, and detect cracks. However, none of these works studies the global mapping of cracks, corrosion, delamination and elastic modulus of the bridge decks based on NDE technologies. Difference to all of the above mentioned works, in this paper we focus on the development of a real world practical robotic system which integrates advanced NDE technologies for the bridge deck data collection. Compared to the current manual data collection technologies, the developed robotic system can reduce the cost and time of the bridge deck data collection. Also, there is no safety risks since the robot can autonomously travel and collect data on the bridge deck without human operators. Moreover, advanced data analysis algorithms are proposed by taking into account the advantages of the accurate robotic localization and navigation to provide the high resolution bridge deck image, crack map, corrosion, delamination and elastic modulus maps of the deck.

### B. Challenges

In our proposed robotic system, accurate localization and navigation algorithms [11] are implemented. The high resolution images, electrical resistivity (ER), impact-echo (IE) and ultrasonic surface waves (USW) data are collected at every certain distance on the deck then stored in the onboard robot computers as well as wirelessly transferred to the command center on the van for online data processing. To implement this system and generate condition maps of the deck, there are several challenging problems that should be addressed.

- Crack Detection and Mapping: Unlike cracks on the pavement surface which are commonly distinct from the background, the cracks on concrete deck surfaces are surrounded by the background image clutter. This difference makes many reported vision-based algorithms [12], [13] difficult to be directly applied to the concrete bridge deck crack detection. In this paper, we take a special consideration of the noisy image of the bridge deck surface and present an effective crack detection and mapping approach.

This work was supported by the Federal Highway Administration within the Long Term Bridge Performance (LTBP) Program

Hung La is with the Department of Computer Science and Engineering, University of Nevada, Reno, NV 89557, USA, email: hla@unr.edu

Nenad Gucunski is with the Department of Civil and Environmental Engineering, Rutgers University, Piscataway, NJ 08854, USA, email: gucunski@rci.rutgers.edu

Seong-Hoon Kee is with the Department of Architectural Engineering, Dong-A University, Busan, Korea, email: shkee@dau.ac.kr

Jingang Yi is with the Department of Mechanical and Aerospace Engineering, Rutgers University, Piscataway, NJ 08854, USA, email: jgyi@rutgers.edu

Turgay Senlet and Luan Nguyen are with the Department of Computer Science, Rutgers University, Piscataway, NJ 08854, USA, emails: tsenlet@cs.rutgers.edu, lvn12@cs.rutgers.edu

- Bridge Deck Condition Mapping: To efficiently inspect the quality of the deck, the corrosion, delamination and elastic modulus mapping should be obtained. The corrosion map provides the corrosive environment of the deck. The delamination and modulus maps provide the horizontal crack areas (with respect to the depth, spread and severity) and the indicators of the strength of the bridge deck. In order to build these condition maps, the robot has to obtain electrical resistivity (ER), impact-echo (IE) and ultrasonic surface waves (USW) measurements on a very dense test grid (e.g. every 60 cm), and this requires accurate localization and navigation for the robot. Additionally, since these IE and USW raw measurement data usually consists of noise, the filter and Fourier transformation should be applied to extract useful information for map interpreting.

The paper is organized as follows. In the next section, we briefly describe the robotic NDE system. In Section III, we present the crack detection and mapping algorithm. The ER, IE and USW data analysis and mapping are presented in Section IV. The testing results are presented in Section V. Finally, the conclusion of the paper is given in Section VI.

## II. THE ROBOTIC NDE SYSTEMS FOR BRIDGE DECK INSPECTION AND EVALUATION

### A. Robotic NDE system

Fig. 1 shows the autonomous robotic NDE system. The mobile platform is a Seekur robot from Adept Mobile Robot Inc. The mobile robot has been significantly modified and equipped with various sensors, actuators, and computing devices. The navigation and motion planning sensors include two RTK GPS units (from Novatel Inc.), one front- and two side-mounted laser scanners (from Sick AG and Hokuyo Automation Co., respectively), and one IMU sensor (from Microstrain Inc.) The onboard NDE sensors include two ground penetration radar (GPR) arrays, two seismic/acoustic sensor arrays, four electrical resistivity (Wenner) probes, two high-resolution surface imaging cameras and a 360-degree panoramic camera. The details of the system are provided in [11], [14].

Three embedded computers (from Versalogic Inc.) are installed inside the robot. One computer runs Robotic Operating System (ROS) nodes for the robot navigation and motion planning tasks. The other two computers are used for the NDE sensors integration and data collection. High-speed Ethernet connections are used among these computers. The NDE data are transmitted in real-time to the remote computers for visualization and data analysis purposes (see Fig. 2). A set of mechatronic systems are used to integrate the NDE sensors with the mobile robot [11]. For example, the seismic/acoustic sensor arrays and electrical resistivity probes need to be in contact with the deck surface for the measurement. To accomplish it, a pair of pneumatic actuators were built to move these NDE sensors up from and down to the deck surface at a predefined distances (e.g., 0.6m) for data collection.

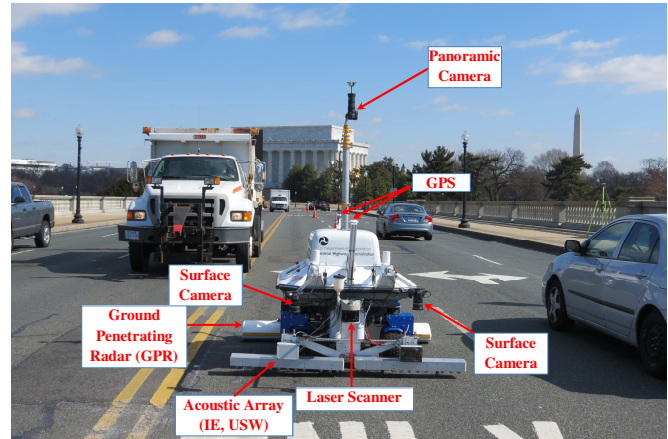


Fig. 1. The deployment of the robotic NDE bridge deck inspection system on the Arlington Memorial bridge, Washington DC, USA in 2013.

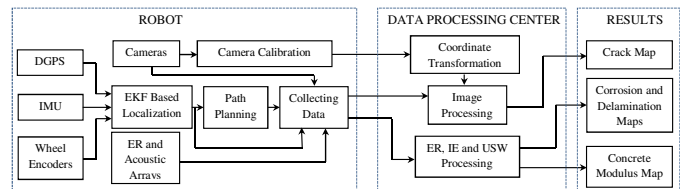


Fig. 2. The working principle of the robotic bridge deck inspection system.

The two facing-down surface cameras (Canon EOS Rebel T3i, 16 MPixel) are mounted on two computer-controlled pneumatic rods. The resolution of the cameras is up to  $5184 \times 3456$  pixels. These two surface cameras are extended out of the robot footprint area when the robot starts the data collection. Each of the cameras covers an area of a size of  $1.83m \times 0.6m$ . The images simultaneously collected by these two cameras have a about 30% overlap area that is used for image stitching.

### B. Robot motion planning for bridge deck inspection

To conduct the NDE data collection, the robot navigates on the bridge deck and collects data lane by lane. As mentioned above, a common practice for collecting the NDE data is to conduct the stop-and-go motion at a certain distance. When the robot stops to collect the NDE data, the two surface cameras also take images of the deck surface. A highly-accurate robot localization and navigation is critical for a successful data collection and inspection. In [11], [14], we have presented an extended Kalman filter (EKF)-based design to fuse the wheel encoder, onboard inertial measurement unit (IMU) and a high-performance global positioning system (GPS) for robot localization and navigation.

The robot motion planning and control is presented in [11] and we briefly discuss here for presentation convenience for the crack detection and mapping algorithms in the next section. Fig. 3 illustrates the robot navigation scheme during the bridge deck inspection. For a straightline bridge, the bridge deck area is of a rectangular shape. To cover the

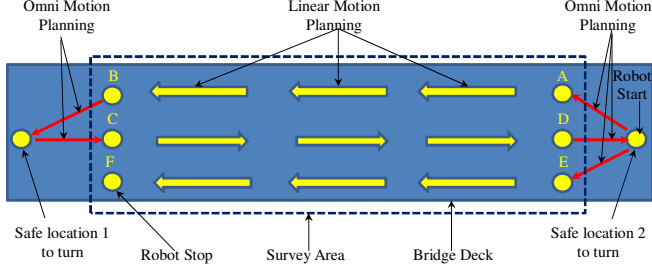


Fig. 3. Schematic of the robot motion planning on the bridge deck.

desired deck area as shown in Fig. 3, three GPS points are first obtained at the rectangle corners such as points  $A$ ,  $E$ , and  $F$ . Using the GPS points of these three corners, the zigzag-shape robot motion trajectories (with interpolated waypoints  $B$ ,  $C$ , and  $D$ ) are computed by the trapezoidal decomposition algorithm, as the arrows indicate in the figure. The robot motion to cover the inspection area consists of linear and omni trajectories. The linear motion allows the robot to follow the straight-line precisely to collect the image and NDE data. At the end of each straightline, the omni-motion is used to navigate the robot safely and to turn around sharply. With these planned trajectories, a potential function-based approach is designed for robot motion control [11].

### III. CRACK DETECTION ALGORITHM

A major difference between the crack appearance on a concrete bridge deck surface and an asphalt pavement surface is that the former has much more noisy background than the latter one. Fig. 4 shows an example of the comparison of two crack images on the concrete and the asphalt surfaces. There are many blebs and steins surround the crack area on the concrete deck surfaces. This example clearly demonstrates the challenging aspect to detect the cracks on bridge deck surfaces.

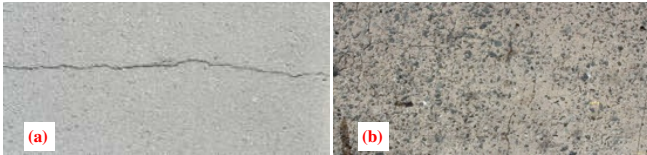


Fig. 4. (a) Crack on an asphalt surface. The crack is very distinct from the background. (b) Cracks on a concrete bridge deck surface. The cracks are surrounded by image clutter.

Because of the abovementioned challenge, the commonly used edge/crack detection methods such as Canny or Laplace of Gaussian (LoG) [15] cannot successfully detect the cracks. We propose a crack detection algorithm with steps shown in Fig. 5. In the following, we describe three major steps in the algorithm: crack detection, crack linking and noise removal.

1) *Gradient crack/edge detection*: The goal of the crack detection module is to identify and quantify the possible crack pixels and their orientations. Let  $I(x, y)$  be the source

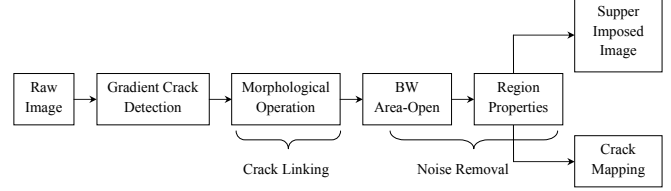


Fig. 5. Flowchart of the crack detection algorithm.

image at pixel  $(x, y)$ . We calculate the gradient vector of the intensity  $I(x, y)$  as

$$\mathbf{I}_g = \nabla I(x, y) = \frac{\partial I}{\partial x} \mathbf{i} + \frac{\partial I}{\partial y} \mathbf{j} = I_x \mathbf{i} + I_y \mathbf{j}, \quad (1)$$

where  $I_x = \frac{\partial I}{\partial x}$  and  $I_y = \frac{\partial I}{\partial y}$  and  $(\mathbf{i}, \mathbf{j})$  are the gradient elements and unit vectors along the  $x$ - and  $y$ -axis directions, respectively. We refine and extend the above gradient operator (1) by considering the edge/crack orientation in the diagonal directions besides the horizontal ( $x$ -axis) and vertical ( $y$ -axis) directions. We introduce eight gradient kernels to compute the gradients of  $I(x, y)$ . The eight  $3 \times 3$  convolution kernels  $\mathbf{L}_\theta$ ,  $\theta = \frac{\pi}{4}k$ ,  $k = 0, \dots, 7$ , are defined in (2) on the top of the next page and  $\mathbf{L}_{\frac{4\pi}{4}} = \mathbf{L}_{\frac{2\pi}{4}}^T$ ,  $\mathbf{L}_{\frac{5\pi}{4}} = \mathbf{L}_{\frac{\pi}{4}}^T$  and  $\mathbf{L}_{\frac{6\pi}{4}} = \mathbf{L}_{\frac{3\pi}{4}}^T$ . By calculating the convolution  $I(x, y) * \mathbf{L}_\theta$ , we obtain an approximation of the gradient/derivatives of the image intensity function (1) along the orientation  $\theta$ . These kernels are applied separately to the input image, to produce separate measurements of the gradient component in each orientation. These calculations are also combined together to find the absolute magnitude of the gradient at each point and the orientation of that gradient. Fig. 6(b) shows an example of the result of the gradient edge/crack detection for a bridge deck surface image shown in Fig. 6(a).

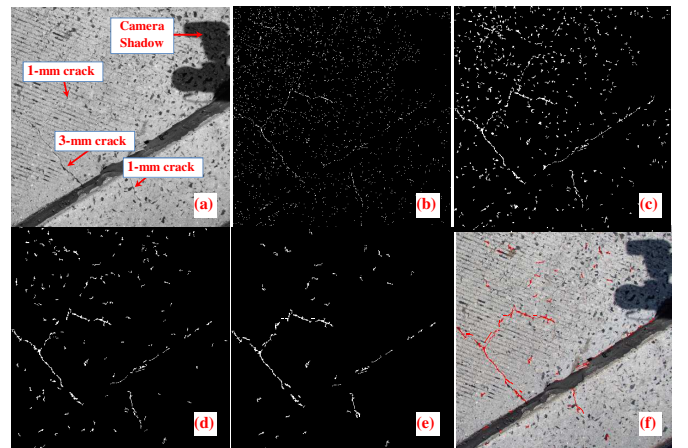


Fig. 6. Crack detection procedure: (a) Original image with different small crack sizes (1mm, 2mm and 3mm) taken at a bridge in New Jersey; (b) Cracks are detected by gradient-based edge detection; (c) After applying edge cleaning and linking process; (d) After applying noise filters; (e) Final crack detection; (f) Crack are superimposed with the image.

2) *Crack/edge cleaning and linking*: After applying the gradient crack detection process, a crack cleaning and linking

$$\mathbf{L}_0 = \begin{bmatrix} 1 & 0 & -1 \\ 1 & 0 & -1 \\ 1 & 0 & -1 \end{bmatrix}, \mathbf{L}_{\frac{\pi}{4}} = \begin{bmatrix} 0 & -1 & -1 \\ 1 & 0 & -1 \\ 1 & 1 & 0 \end{bmatrix}, \mathbf{L}_{\frac{2\pi}{4}} = \begin{bmatrix} -1 & -1 & -1 \\ 0 & 0 & 0 \\ 1 & 1 & 1 \end{bmatrix}, \mathbf{L}_{\frac{3\pi}{4}} = \begin{bmatrix} -1 & -1 & 0 \\ -1 & 0 & 1 \\ 0 & 1 & 1 \end{bmatrix}, \mathbf{L}_{\frac{7\pi}{4}} = \begin{bmatrix} 1 & 1 & 0 \\ 1 & 0 & 1 \\ 0 & -1 & -1 \end{bmatrix}, \quad (2)$$

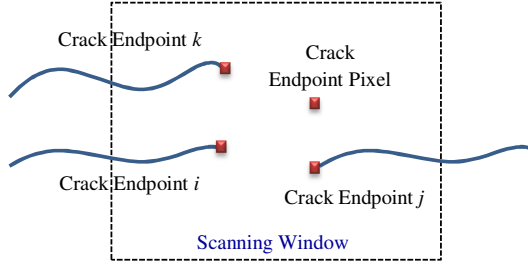


Fig. 7. Schematic of identifying the linking crack path to the  $j$ th crack path.

process is applied to remove noise and link the crack pixels to form a continuous crack. Crack cleaning is performed via the Morphological operation. These operations can remove isolated pixels and link pixels in the small neighborhood windows if most pixels in these windows are the crack pixels.

In the crack linking process, the first step is to identify the starting and the ending points of the crack. Once this step is established, the crack linking process defines the scanning window size and then determines the maximum linking distance. To decide the linking direction, similar to the approach in [16] a cost function for the  $j$ th crack path is defined as

$$F_j(i) = K_p \sqrt{(x_{ep}^i - x_{ep}^j)^2 + (y_{ep}^i - y_{ep}^j)^2} + K_d, \quad (3)$$

for any  $i$ th crack in the scanning window area, where  $(x_{ep}^i, y_{ep}^i)$  and  $(x_{ep}^j, y_{ep}^j)$  are the crack end-point locations of the  $i$ th and  $j$ th crack paths, respectively; see Fig. 7. Parameters  $K_p$  and  $K_d$  are constants that will be experimentally determined. After calculating  $F_j(i)$  for all cracks in the scanning window, the minimum value of the cost function,  $i^* = \arg \min_i F_j(i)$ , determines the  $i^*$ th crack path to be linked to the  $j$ th crack path. Fig. 6(c) shows the example of the crack linking result.

3) *Noise removal*: We first remove small noisy connected components which have fewer than certain pixels in the area of two-dimensional eight-connected neighborhood. Fig. 6(d) shows the example of the result by using these noise removal actions.

We developed a process to further remove noise pixels by looking at crack area. Let  $(x_c^i, y_c^i)$  be the center location of the  $i$ th crack region in the crack area. We first compute the distance among these crack regions as

$$d(i, j) = \sqrt{(x_c^i - x_c^j)^2 + (y_c^i - y_c^j)^2}, i, j = 1, \dots, N_c, \quad (4)$$

where  $N_c$  is the total number of centroids of the crack regions. We then combine the calculated distances  $d(i, j)$

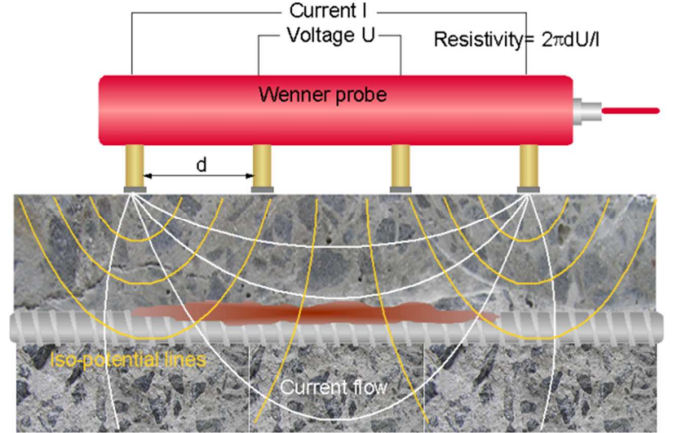


Fig. 8. Principle of electrical resistivity (ER) measurement using Wenner probe.

and the total areas  $A(i)$  for the  $i$ th crack region to remove noises. The crack area  $A(i)$  is calculated by the total number of pixels covered by detected  $i$ th crack region. With known  $d(i, j)$  and  $A(i)$ , we compare their values with the predefined thresholds  $T_d$  and  $T_a$ , respectively. If both the values of  $d(i, j)$  and  $A(i)$  are smaller than these thresholds, then  $i$ th crack region is removed from the detected candidate pool. Comparing with the result in Fig. 6(d), Fig. 6(e) shows the further cleaning result and final crack detection results.

## IV. NDE DATA COLLECTION AND ANALYSIS

### A. Electrical Resistivity Data Analysis

The corrosive environment of concrete and thus potential for corrosion of reinforcing steel can be well evaluated through measurement of ER of concrete. Dry concrete will pose a high resistance to the passage of current, and thus will be unable to support ionic flow. On the other hand, presence of water and chlorides in concrete, and increased porosity due to damage and cracks, will increase ion flow, and thus reduce resistivity. It has been observed that a resistivity less than 5 k $\Omega$  can support very rapid corrosion of steel. In contrast, dry concrete may have resistivity above 100 k $\Omega$ . Research has shown in a number of cases that ER of concrete can be related to the corrosion rates of reinforcing steel. The ER surveys are commonly conducted using a four-electrode Wenner probe, as illustrated in Figure 8. Electrical current is applied through two outer electrodes, while the potential of the generated electrical field is measured using two inner electrodes. From the two, ER is calculated as indicated in Figure 8.

### B. Impact-Echo (IE) Data Analysis

Impact-Echo (IE) is a widely used NDT (nondestructive testing) method that has demonstrated to be effective in identifying and characterizing delaminations in concrete structures. Impact-Echo (IE) is an elastic-wave based method to identify and characterize delaminations in concrete structures. This method uses the transient vibration response of a plate-like structure subjected to a mechanical impact. The mechanical impact generates body waves (P-waves or longitudinal waves and S-waves or transverse waves), and surface-guided waves (e.g. Lamb and Rayleigh surface waves) that propagate in the plate. The multiple-reflected and mode-converted body waves eventually construct infinite sets of vibration resonance modes within the plate. In practice, the transient time response of the solid structure is commonly measured with a contact sensor (e.g., a displacement sensor or accelerometer) coupled to the surface close to the impact source. The Fourier transform (amplitude spectrum) of the measured transient time-signal is applied to find the maxima (peaks) at certain frequencies, which represent particular resonance modes.

### C. Ultrasonic Surface Waves (USW) Data Analysis

The ultrasonic surface waves (USW) technique is an offshoot of the spectral analysis of surface waves (SASW) method used to evaluate material properties (elastic moduli) in the near-surface zone. The SASW uses the phenomenon of surface wave dispersion (i.e., velocity of propagation as a function of frequency and wave length, in layered systems to obtain the information about layer thickness and elastic moduli). The USW test is identical to the SASW, except that the frequency range of interest is limited to a narrow high-frequency range in which the surface wave penetration depth does not exceed the thickness of the tested object. In cases of relatively homogeneous materials, the velocity of the surface waves does not vary significantly with frequency. The surface wave velocity can be precisely related

### D. Data Representation

To present test data and results in an effective and intuitive manner, the results of the NDE surveys using the above mentioned three technologies are presented by two-dimensional contour maps (Fig. 10). On each contour map, the location of joints are marked as white lines at both ends in order to better identify dimensions of the bridges and locations of deterioration. Condition ratings with respect to delamination (IE) and corrosion (ER) for the section of the bridge surveyed were calculated on a scale 0 (worst) to 100 (best). Three different weight factors (100, 70, 40) are assigned to the area in different conditions and delamination and corrosion rates for each bridge which are calculated by delamination rating ( $D_r$ ) and corrosion rating ( $C_r$ ) in (5, 6).

$$D_r = \frac{100 * A_{good} + 70 * A_{fair} + 40 * A_{poor}}{A_{total}} \quad (5)$$

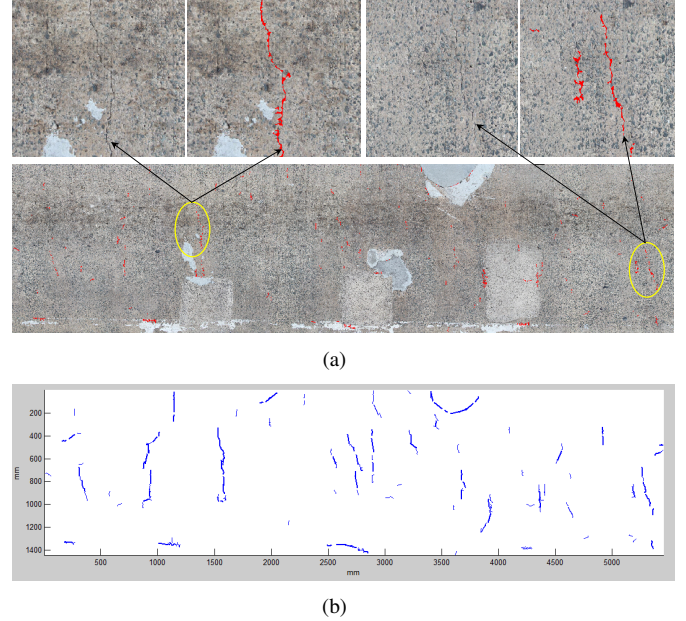


Fig. 9. Crack detection and mapping results for a bridge deck area on the Haymarket bridge in Virginia in June 2013. (a) Stitched image from robotic collected images with several crack samples. (b) Crack map with crack sizes and lengths.

where  $A_{good}$ ,  $A_{fair}$ ,  $A_{poor}$  are the areas in “Good”, “Fair”, and “Poor” conditions, respectively, which are described as follows:

- Good condition is established by measuring strong reflections from the bottom of the deck;
- Fair condition is characterized by shallow depth delamination induced reflections, causing a shift in the response spectrum towards higher frequencies;
- Poor condition is characterized by a single peak at a frequency corresponding to the depth of the delamination;
- Serious condition is evidenced by a low frequency response of flexural mode oscillations of the upper, delaminated, portion of the deck.

$$C_r = \frac{100 * A_{low} + 70 * A_{moderate} + 40 * A_{high}}{A_{total}} \quad (6)$$

where  $A_{low}$ ,  $A_{moderate}$ ,  $A_{high}$  are the areas with ER in their ranges of: 0-25 k $\Omega$ , 25-40 k $\Omega$ , and greater than 40 k $\Omega$ , respectively, and  $A_{total}$  is the total surveyed area.

## V. DEPLOYMENT RESULTS

The proposed robotic system has been deployed on more than 30 bridges in New Jersey, Virginia, Washington DC, Maryland and Illinois, etc. Due to the page limit, we here present the results of couple bridges.

Fig. 9(a) shows the images stitched over an area of a size of 5.5m  $\times$  1.45m. Crack detection is performed in this stitched image. The top sub-figures are the zoom-in images at several crack locations for clear presentation and demonstration. Fig. 9(b) shows the crack detection and mapping results for the same bridge deck area shown in Fig. 9(a). Crack map is

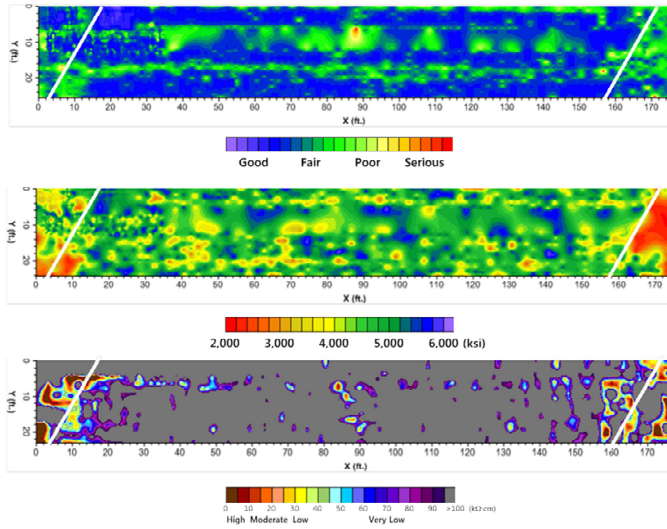


Fig. 10. Condition maps for a bridge deck in Illinois state in April 2014, USA: (Top) The impact-echo (IE); (Middle) The ultrasonic surface waves (USW); (Bottom) The electrical resistivity (ER). The robot covers a half of the bridge with three scans (6ft width/scan) and 175ft along within 50 minutes.

built on the results from robot navigation and motion control results presented in Section II.

The crack detection and mapping results not only localize the cracks on the bridge but also provide the sizes of these cracks. Table I lists the statistics of the detected cracks on the bridge deck area. From these calculations, we automatically obtain various statistical and location information about the cracks and their properties, which are both critical for quality assessment of the bridge deck.

TABLE I  
STATISTICS OF THE DETECTED CRACKS FOR THE BRIDGE DECK AREA SHOWN IN FIG. 9(A)

|                 | Total  | Longest    | Shortest    | Max. width  | Min. width |
|-----------------|--------|------------|-------------|-------------|------------|
| Length          | 10.6 m | 70 cm      | 5 cm        | 1.5 cm      | 1.5 mm     |
| Loc. (x, y) (m) | N/A    | (1.6, 0.7) | (5.5, 1.22) | (5.45, 1.1) | (4.2, 7.1) |

The results of the NDE surveys using IE, USW, and ER for a bridge in Illinois state are presented as contour maps in Figure 10, respectively. Delamination condition ratings, concrete modulus, and corrosion ratings can be observed in this figure. We can see that the deck is in a good condition with respect to delamination since there are only a few spots in poor or serious conditions. According to the condition maps for concrete quality, many small spots and some large areas with the modulus less than 3,000 ksi were observed, especially at both ends of the surveyed areas. The mean and standard deviation of the concrete modulus are 4,582 ksi and 926 ksi which indicate that the large variation in the concrete modulus of this bridge. In terms of the corrosion rate, overall good condition was identified throughout the scanned bridge deck. Although several locations where moderate to high

corrosion probability were found.

## VI. CONCLUSIONS

A new development of the high efficiency robotic system for bridge deck data collection and analysis has been reported. Several challenging problems of crack detection and mapping, ER, IE and USW analysis have been tackled. The advanced crack detection and mapping algorithm allowed to detect cracks accurately in high noisy concrete images and build the whole crack map of the deck. The corrosion, delamination and elastic modulus maps were built based on ER, IE and USW data collected by the robot to provide easy evaluation and monitor of the bridge. Extensive testings and deployments of the proposed robotic system on many bridges proved the efficiency of the new approach for bridge deck inspection and evaluation.

## REFERENCES

- [1] ASCE. 2009 Report Card for Americas Infrastructure. Technical report, American Society of Civil Engineers, 2009.
- [2] S. A. Velinsky. Heavy vehicle system for automated pavement crack sealing. *Int. J. Veh. Design*, 1(1):114–128, 1993.
- [3] S. J. Lorenc and B. E. Handlon and L. E. Bernold. Development of a robotic bridge maintenance system. *Automat. Constr.*, 9:251–258, 2000.
- [4] S. N. Yu, J. H. Jang, and C. S. Han. Auto inspection system using a mobile robot for detecting concrete cracks in a tunnel. *Automat. Constr.*, 16:255–261, 2007.
- [5] P. C. Tung, Y. R. Hwang, and M. C. Wu. The development of a mobile manipulator imaging system for bridge crack inspection. *Automat. Constr.*, 11:717–729, 2002.
- [6] J. H. Lee, J. M. Lee, J. W. Park, and Y. S. Moon. Efficient algorithms for automatic detection of cracks on a concrete bridge. In *Proc. 23rd Int. Tech. Conf. Circ./Syst., Comp. Communicat.*, pages 1213–1216, Yamaguchi, Japan, 2008.
- [7] J. K. Oh, G. Jang, S. Oh, J. H. Lee, B. J. Yi, Y. S. Moon, J. S. Lee, and Y. Choi. Bridge inspection robot system with machine vision. *Automat. Constr.*, 18:929–941, 2009.
- [8] R. S. Lim, H. M. La, Z. Shan, and W. Sheng. Developing a crack inspection robot for bridge maintenance. In *Proc. IEEE Int. Conf. Robot. Autom.*, pages 6288–6293, Shanghai, China, 2011.
- [9] R. S. Lim, H. M. La, and W. Sheng. A robotic crack inspection and mapping system for bridge deck maintenance. *IEEE Trans. on Automat. Sci. and Eng.*, 11(2):367–378, Apr. 2014.
- [10] S.-N. Yu, J.-H. Jang, and C.-S. Han. Auto inspection system using a mobile robot for detecting concrete cracks in a tunnel. *Automat. Constr.*, 16:255–261, 2007.
- [11] H. M. La, R. S. Lim, B. B. Basily, N. Gucunski, J. Yi, A. Maher, F. A. Romero, and H. Parvardeh. Mechatronic systems design for an autonomous robotic system for high-efficiency bridge deck inspection and evaluation. *IEEE/ASME Trans. Mechatronics*, 18(6):1655–1664, 2013.
- [12] Y. Fujita and Y. Hamamoto. A robust automatic crack detection method from noisy concrete surfaces. *Machine Vision and Applications*, 22:245–254, 2011.
- [13] T. Nishikawa, J. Yoshida, and T. Sugiyama. Concrete crack detection by multiple sequential image filtering. *Computer-Aided Civil and Infrast. Eng.*, 27:29–47, 2012.
- [14] H. La, R. Lim, B. Basily, N. Gucunski, J. Yi, A. Maher, F. Romero, and H. Parvardeh. Autonomous robotic system for high-efficiency non-destructive bridge deck inspection and evaluation. In *Proc. IEEE Conf. Automat. Sci. Eng.*, pages 1065–1070, Madison, WI, 2013.
- [15] D. A. Forsyth and J. Ponce. *Computer Vision: A Modern Approach*. Prentice Hall, Upper Saddle River, NJ, 2003.
- [16] O. Ghita and P. F. Whelan. Computational approach for edge linking. *J. Elect. Imaging*, 4(11):479–485, 2002.